Title

Domain-Swap Dimerization of Acanthamoeba castellanii CYP51 and a Unique Mechanism of Inactivation by Isavuconazole.

Journal

Molecular Pharmacology, 98(6)

Authors

Sharma, Vandna

Shing, Brian

Hernandez-Alvarez, Lilian

et al.

Publication Date

2020-12-01

DOI

10.1124/molpharm.120.000092

Peer reviewed

1521-0111/98/6/770–780$35.00
MOLECULAR PHARMACOLOGY

https://doi.org/10.1124/molpharm.120.000092
Mol Pharmacol 98:770–780, December 2020

Domain-Swap Dimerization of *Acanthamoeba castellanii* CYP51 and a Unique Mechanism of Inactivation by Isavuconazole[S]

Vandna Sharma, Brian Shing, Lilian Hernandez-Alvarez, Anjan Debnath, and Larissa M. Podust

Skaggs School of Pharmacy and Pharmaceutical Sciences, Center for Discovery and Innovation in Parasitic Diseases, University of California San Diego, La Jolla, California (V.S., B.S., L.H.-A., A.D., L.M.P.) and Departamento de Física, Instituto de Biociências, Letras e Ciências Exatas, Universidade Estadual Paulista Julio de Mesquita Filho, São José do Rio Preto, São Paulo, Brazil (L.H.-A.)

Received June 14, 2020; accepted September 17, 2020

ABSTRACT

Cytochromes P450 (P450, CYP) metabolize a wide variety of endogenous and exogenous lipophilic molecules, including most drugs. Sterol 14α-demethylase (CYP51) is a target for antifungal drugs known as conazoles. Using X-ray crystallography, we have discovered a domain-swap homodimerization mode in CYP51 from a human pathogen, *Acanthamoeba castellanii* CYP51 (AcCYP51). Recombinant AcCYP51 with a truncated transmembrane helix was purified as a heterogeneous mixture corresponding to the dimer and monomer units. Spectral analyses of these two populations have shown that the CO-bound ferrous form of the dimeric protein absorbed at 448 nm (catalytically competent form), whereas the monomeric form absorbed at 420 nm (catalytically incompetent form). AcCYP51 dimerized head-to-head via N-termini swapping, resulting in formation of a nonplanar protein-protein interface exceeding 2000 Å^2 with a total solvation energy gain of −35.4 kcal/mol. In the dimer, the protomers faced each other through the F and G α-helices, thus blocking the substrate access channel. In the presence of the drugs clotrimazole and isavuconazole, the AcCYP51 drug complexes crystallized as monomers. Although clotrimazole-bound AcCYP51 adopted a typical CYP monomer structure, isavuconazole-bound AcCYP51 failed to refold 74 N-terminal residues. The failure of AcCYP51 to fully refold upon inhibitor binding in vivo would cause an irreversible loss of a structurally aberrant enzyme through proteolytic degradation. This assumption explains the superior potency of isavuconazole against *A. castellanii*. The dimerization mode observed in this work is compatible with membrane association and may be relevant to other members of the CYP family of biologic, medical, and pharmacological importance.

SIGNIFICANCE STATEMENT

We investigated the mechanism of action of antifungal drugs in the human pathogen *Acanthamoeba castellanii*. We discovered that the enzyme target [*Acanthamoeba castellanii* sterol 14α-demethylase (AcCYP51)] formed a dimer via an N-termini swap, whereas drug-bound AcCYP51 was monomeric. In the AcCYP51-isavuconazole complex, the protein target failed to refold 74 N-terminal residues, suggesting a fundamentally different mechanism of AcCYP51 inactivation than only blocking the active site. Proteolytic degradation of a structurally aberrant enzyme would explain the superior potency of isavuconazole against *A. castellanii*.

Introduction

Acanthamoeba is a water- and soil-dwelling amoeba and an opportunistic pathogen of clinical interest. It is responsible for several diseases in humans, involving infections of the eye, brain, and skin (Marciano-Cabral and Cabral, 2003). *Acanthamoeba* has two distinct stages: trophozoite and cyst (Siddiqui and Khan, 2012). Sterol 14α-demethylase (CYP51) in *Acanthamoeba castellanii* is an essential enzyme in the biosynthesis of ergosterol, a functional analog of cholesterol in mammalian cells (Lamb et al., 2015; Thomson et al., 2017). CYP51 is a validated drug target in fungi and emerging drug target in the eukaryotic human pathogens (Choi et al., 2014b), including *Trypanosoma cruzi* (Choi et al., 2013, 2014a,b; Calvet et al., 2014; Vieira et al., 2014a,b), *Naegleria fowleri* (Debnath et al., 2017; Zhou et al., 2018), and *Acanthamoeba*

L.M.P. was supported by start-up fund of the University of California San Diego, the University of California San Diego Center for Tropical Diseases fund, and the University of California San Diego Academic Senate grant. A.D. was supported by National Institutes of Health National Center for Advancing Translational Sciences [Grant 1KL2-TR001444] and National Institute of Allergy and Infectious Diseases [Grants R21 AI133394, R21 AI141210, and R21 AI146460]. L.H.-A. was supported by São Paulo Research Foundation Agency (FAPESP) [Grant 2018/25311-2]. This research used resources of the Advanced Light Source, which is a Department of Energy (DOE) Office of Science User Facility under contract DE-AC02-05CH11231. The atomic coordinates and structure factors (6Q2C, 6UX0, and 6UW2) have been deposited in the Protein Data Bank, Research Collaboratory for Structural Bioinformatics, Rutgers University, New Brunswick, NJ (http://www.rcsb.org/).

Competing interests: There is no financial and nonfinancial competing interests.

https://doi.org/10.1124/molpharm.120.000092.

[S] This article has supplemental material available at molpharm.aspetjournals.org.

ABBREVIATIONS: AcCYP51, *Acanthamoeba castellanii* sterol 14α-demethylase; CYP51, sterol 14α-demethylase; ER, endoplasmic reticulum; MALS, multiangle light scattering; MD, molecular dynamics; MM, molecular mass; NTA, nitrilotriacetic acid; P420, cytochrome P420; P450, cytochrome P450; PDB, Protein Data Bank; POPC, 1-palmitoyl-2-oleoyl-*sn*-glycero-3-phosphocholine; POPE, 1-palmitoyl-2-oleoyl-*sn*-glycero-3-phosphoethanolamine; SEC-MALS, size-exclusion chromatography–MALS; TM, transmembrane.

(Thomson et al., 2017; Zhou et al., 2019; Shing et al., 2020). Repurposing of the antifungal azole drugs targeting CYP51 (known as conazoles) is a promising strategy to combat *Acanthamoeba* infections (Thomson et al., 2017; Zhou et al., 2019; Shing et al., 2020).

The majority of antifungal conazoles have submicromolar or low micromolar potency against *Acanthamoeba* in cell-based assays (Lamb et al., 2015; Martín-Navarro et al., 2015; Thomson et al., 2017). However, the activity of isavuconazole against proliferating trophozoites is superior to both standard anti-*Acanthamoeba* therapy and other conazole drugs (Shing et al., 2020). Depending on the *A. castellanii* strain, isavuconazole potency varies in different strains from 26 nM (MEEI 0184) to 4.6 nM (Ma) to <1 nM (CDC:V240) (Shing et al., 2020). Against the *A. castellanii* Ma strain, isavuconazole potency (EC_{50} of 4.6 nM) was one order of magnitude higher than that of posaconazole (EC_{50} of 44.5 nM) or clotrimazole (EC_{50} of 200 nM) (Shing et al., 2020). Furthermore, isavuconazole at 70 μM completely prevented excystation of viable *Acanthamoeba* cysts (Shing et al., 2020). Potency against both trophozoite and cyst makes isavuconazole a promising drug candidate to block the propagation of trophozoite–cyst cycling of *Acanthamoeba* in *Acanthamoeba* keratitis.

In the context of our drug discovery and drug repurposing efforts, we pursued elucidation of the drug-target interactions for inhibitors targeting *Acanthamoeba castellanii* CYP51 (AcCYP51). In the course of these studies, we have observed an unusual property of AcCYP51 to form a stable dimer that sustained size-exclusion chromatography during purification. As we discovered subsequently, the dimerization occurred via a domain-swap mechanism through the exchange of the N-terminal regions between two protomers. Domain swapping has not been reported in CYP protein family P450 previously. In this article, we use abbreviation CYP to denote a P450 protein family, while P450 term is reserved for the ferrous CO-bound form with iron Soret band at ∼450 nm in order to distinguish it from the P420 form. The recombinant CYP enzymes of bacterial origin are monomeric, whereas CYP enzymes of higher eukaryotes, when expressed heterologously, tend to form random aggregates in solution, and their multimolecular assemblies have been detected in crystal structures (Reed and Backes, 2017).

At physiologic conditions, endoplasmic reticulum (ER)-bound CYP enzymes presumably exist as homo- or even hetero-oligomers. The fluorescence resonance energy transfer and bimolecular fluorescence complementation in living cells suggest that CYP2C2 forms homo-oligomers and that the homo-oligomerization is dependent on the signal membrane anchor sequence (Szczesna-Skorupa et al., 2003; Ozalp et al., 2005). Homodimerization in intact cellular membranes was suggested for the steroidogenic CYP17 and CYP19 by fluorescence resonance energy transfer coupled with quartz crystal microbalance and atomic force microscopy (Praporski et al., 2009). Homodimerization for the drug-metabolizing CYP2C8 was demonstrated by cysteine-scanning mutagenesis and crosslinking of sulfhydryl groups (Hu et al., 2010). Finally, homo- and hetero-oligomerization in microsomal membranes was demonstrated for CYP3A4, CYP3A5, and CYP2E1 by luminescence resonance energy transfer (Davydov et al., 2015). Despite these biophysical and biochemical observations, the CYP oligomerization mode is unknown. The random intermolecular protein-protein interfaces observed crystallographically are heterogeneous and planar and have a relatively small interaction area ranging from 290 to 550 $Å^2$ (Scott et al., 2003; Schoch et al., 2004; Ouellet et al., 2008; Reed and Backes, 2017).

In this work, we have structurally characterized CYP51 from the lower eukaryote *A. castellanii* strain Neff (AcCYP51), which is expressed with a truncated transmembrane helix. We found that only dimeric AcCYP51 had spectral characteristics typical of the functionally competent CYP enzymes. By X-ray crystallography, we demonstrated that AcCYP51 alone is dimerized via N-termini swapping, resulting in formation of a 2000 $Å^2$ nonplanar protein-protein interface. When bound to the azole inhibitors clotrimazole and isavuconazole, AcCYP51 crystallized in the monomeric form with the 74 N-terminal residues disordered in the AcCYP51-isavuconazole complex. The AcCYP51 X-ray structures confirmed a novel dimerization mechanism and elucidated differences in the clotrimazole- and isavuconazole-binding modes that plausibly explain the superior potency of isavuconazole against *A. castellanii* (Shing et al., 2020).

Materials and Methods

AcCYP51 Expression and Purification

AcCYP51, which is codon-optimized for bacterial expression, had a coding sequence with 42 N-terminal membrane-anchoring residues replaced with the MAKKTSSKGK. A hexahistidine tag was added at the C terminus to increase protein yield and recovery during purification (see Supplemental Data 1). This construct was generated synthetically (GenScript, Piscataway, NJ) and cloned into the pCW-LIC expression vector obtained from the nonprofit plasmid repository (Addgene, Cambridge, MA).

To improve the P450/P420 ratio, the original protocol used to isolate recombinant *N. fowleri* CYP51 (Debnath et al., 2017) was modified (see Supplemental Data 2). Briefly, the modifications included a switch to the HMS174 *Escherichia coli* strain, coexpression of chaperones, omitting detergent 3-[(3-cholamidopropyl)dimethylammonio]-1-propanesulfonate (CHAPS) used initially to facilitate protein release from the membrane, and replacement of imidazole with histidine during elution from the Ni-NTA column. Exposure to imidazole led to quick loss of the 450-nm band in the absorbance spectra of the CO-bound ferrous AcCYP51. Finally, additional purification step of size-exclusion chromatography (SEC) on a Superdex 200 XK 26 column coupled to MALS (SEC-MALS) was used to separate P450 form, which was eluted as a dimer, from P420 form, which was eluted as a monomer. Collectively, after four chromatographic steps, including Ni-NTA affinity chromatography, Q-Sepharose ion-exchange chromatography, hydroxyapatite chromatography, and size-exclusion chromatography, fractions containing AcCYP51 with ∼80% P450 content were pooled, concentrated to ∼1 mM, aliquoted, and frozen at −80°C.

SEC-MALS

SEC-MALS experiments were performed using in-line multiangle light scattering (MALS) detector (miniDAWN; Wyatt Technology, Santa Barbara, CA) at 7°C. Two-milliliter protein sample was injected onto pre-equilibrated Superdex 200 XK26 column using 2-ml sample loop at a flow rate of 0.5 ml/min. The composition of the equilibration and sample buffer used was 50 mM potassium phosphate, pH 8.0, and 5% glycerol. Data of SEC-MALS thus obtained were analyzed by ASTRA 6.1 software provided by the instrument manufacturer.

UV-Visible Analysis of AcCYP51

The spectra were recorded using a Thermo Scientific Multiscan Go UV-visible spectrophotometer. Protein samples were diluted in assay

buffer (50 mM potassium phosphate, pH 8.0, and 10% glycerol) and allowed to equilibrate to room temperature for 10 minutes prior to readings. Spectra were recorded from 250 to 700 nm for the ferric and dithionite-reduced ferrous AcCYP51 in assay cuvette. Baseline was established using buffer alone and was subtracted from the sample signal prior to analysis using SkanIt software provided by the manufacturer. The CO difference spectrum was recorded by placing dithionite-reduced ferrous AcCYP51 into the sample cuvettes and recording the baseline. Then CO was bubbled into the same cuvette, and the difference spectrum was recorded. The concentration of AcCYP51 was approximated from the absorption peak at 450 nm using the extinction coefficient $\varepsilon_{450} = 91\ mM^{-1}cm^{-1}$ (Omura and Sato, 1964).

To assess the spectral properties of the crystallized AcCYP51 dimer, crystals were harvested individually; each crystal was washed thoroughly in a well solution and then dissolved in 50 μl of assay buffer. The number of crystals required for a single analysis varied from 10 to 20 depending on the crystal size. The UV-visible spectra of the dissolved crystals were recorded at ambient temperature in 50-μl cuvette (952010077; Eppendorf). To generate ferrous-CO spectra, a few crystals of sodium dithionite were added to the CO-bubbled ferric protein sample.

Inhibitor Binding by UV-Visible Spectroscopy

Type I and Type II Binding. To determine binding modes of different ligands used in the study, 20-mM ligand stock solutions were prepared in corresponding solvents. Isavuconazole and clotrimazole were prepared in DMSO, and 31-norlenosterol was dissolved in isopropanol. Prior to analysis, 5 μM AcCYP51 in assay buffer was mixed with 20 μM ligand. After 30 minutes of incubation at room temperature, absorbance spectra were recorded from 300 to 500 nm. To determine difference spectra, blank readings were taken for protein alone in assay buffer with respective ligand vehicle under given experimental conditions.

Binding Kinetics. To determine binding kinetics of the ligands, 5 μM AcCYP51 in assay buffer was mixed with 20 μM ligand. After mixing, spectra from 300 to 500 nm were recorded every 5 minutes of incubation. Blank readings were determined from incubation of protein alone with respective ligand vehicle under given experimental conditions. AcCYP51 stock concentration was determined by absorbance of the CO-bound ferrous form at 450 nm ($\varepsilon_{450} = 91\ mM^{-1}cm^{-1}$) (Omura and Sato, 1964). Concentration of the AcCYP51-norlanosterol complex was determined using the peak-to-trough extinction coefficient, $\varepsilon_{390\text{-}420} \approx 100\ mM^{-1}cm^{-1}$) (Luthra et al., 2011). Concentration of the AcCYP51-inhibitor complex was estimated using the peak-to-trough extinction coefficient, $\varepsilon_{430\text{-}411} \approx 110\ mM^{-1}cm^{-1}$) (Wang et al., 2012). The experiment was conducted with two replicates.

Binding Isotherms. The DMSO stock solutions for clotrimazole and isavuconazole were freshly prepared at concentrations of 0.2 and 0.4 mM. The AcCYP51 stock was diluted to 1 μM in assay buffer. Two milliliters of the AcCYP51 solution was split evenly into a reference and a sample cuvette [1-cm polymethyl methacrylate cuvette (cat. no. 759150; BrandTech Scientific, Essex, CT)]. The AcCYP51 solution was allowed to equilibrate for 30 minutes to room temperature prior to absorption readings. The absorption readings were performed at 20°C on a Cary 1E Dual Beam UV-visible spectrophotometer (Varian). The experiment was conducted with two replicates.

In the course of titration, 1 μl of DMSO was added to the reference cuvette, whereas 1 μl of inhibitor dissolved in DMSO was added to the sample cuvette in 200- (data points 1–4) and 400-nM (data points 5–10) increments. The cuvette content was mixed with a transfer pipette prior to each reading. Absorbance readings were taken from 350 to 500 nm, and the binding isotherm was generated by plotting the differences between the absorbance minimum at 410 nm and absorbance maximum at 430 nm as a function of added drug concentration. The data were analyzed in GraphPad Prism 6.07 with the rearrangement of the Morrison binding equation (Morrison, 1969) to determine the dissociation constants:

$$\Delta A = (\Delta A_{max}/\ 2[E])\left((K_D + [L] + [E]) - \left((K_D + [E] + [L])^2 - 4[E][L]\right)^{0.5}\right),$$

in which ΔA is the difference between absorbance maximum and minimum, ΔA_{max} is the extrapolated maximum absorbance difference, [L] is the ligand concentration, and [E] is the enzyme concentration.

Crystallization and Structure Determination

Prior to crystallization, AcCYP51 stored at −80°C in 50 mM potassium phosphate, pH 8.0, and 5% glycerol was diluted 2-fold to 0.5 mM with water or buffer containing a ligand at 1.2 molar access. Screening of crystallization conditions was performed using commercial high-throughput screening kits available in deep-well format from Hampton Research (Aliso Viejo, CA) or Qiagen (Germantown, MD), a nanoliter drop-setting Mosquito robot (TTP LabTech, Melbourn, UK) operating with 96-well plates, and a hanging drop crystallization protocol. For diffraction quality, crystals were further optimized in 96-well plates configured using the Dragonfly robot (TTP LabTech) and the Designer software (TTP LabTech). All crystals were obtained at 23°C. Clotrimazole and isavuconazole stock solutions were prepared fresh in DMSO. The 1:1.2 molar ratio protein-inhibitor mix was incubated for 30 minutes on ice prior to mixing with the well solutions. Optimized crystallization conditions are provided in Table 1.

Diffraction data were collected remotely at beamline 8.3.1, Advanced Light Source, Lawrence Berkeley National Laboratory. Data indexing, integration, and scaling were conducted using XDS (Kabsch, 2010). *T. cruzi* CYP51 structure [sequence identity 38%, Protein Data Bank (PDB): 4C27] was used as a molecular replacement model. The initial AcCYP51 model was built and refined using the BUCCANEER and REFMAC5 modules of the CCP4 software suite (Collaborative Computational Project, Number 4, 1994) and COOT software (Emsley and Cowtan, 2004). Data collection and refinement statistics are shown in Table 1.

Molecular Modeling and Simulation

A full-length AcCYP51 homodimer was constructed computationally by modeling the transmembrane (TM) helix and its flanking regions into the AcCYP51 structure using the Rosetta MP package v3.0 (Koehler Leman et al., 2017). The TM helix (residues 10–30) was modeled ab initio using the helix_from_sequence program (Koehler Leman et al., 2017). The TM helices of each monomer were positioned diagonally opposite one another in agreement with the position of the N termini in the crystal structure. The flexible linker region (residues 31–52) and the N terminus were built for each protomer using the mp_domain_assembly program (Koehler Leman and Bonneau, 2018). Five hundred models were generated, and the structure with the lowest value of the Rosetta energy function was selected for further analysis. The energy minimization of the full-length dimer was performed to optimize interatomic distances and angles. Then, the 50-nanosecond molecular dynamics (MD) simulations were conducted to refine the structure of the linker regions and to obtain the proper arrangement of them in respect to the rest of the dimer. In the course of the simulation, the flexible linkers and the N termini were allowed to move freely, whereas harmonic restraints were applied to the backbone atoms of the rest of the protein.

The fully assembled AcCYP51 dimer was embedded into a 1-palmitoyl-2-oleoyl-*sn*-glycero-3-phosphocholine (POPC)/1-palmitoyl-2-oleoyl-*sn*-glycero-3-phosphoethanolamine (POPE)/cholesterol lipid bilayer composed of 75% POPC, 18% POPE, and 6% cholesterol, corresponding to the abundance of these lipids in the ER (Šrejber et al., 2018). Cholesterol is the closest analog of ergosterol and ergosterol-like lipids in *A. castellanii* membranes available in Amber data base and widely used in Amber force-field simulations. The protein-membrane model

TABLE 1
AcCYP51 structures data collection and refinement statistics

Inhibitor (ID) Oligomerization PDB identification	None Dimer 6Q2C	Clotrimazole (CL6) Monomer 6UW2	Isavuconazole (QKM) Monomer 6UX0
Data collection			
Space group	$P2_12_12_1$	$P2_12_12_1$	P1
Cell dimensions			
a, *b*, *c* (Å)	100.4, 101.6, 123.7	117.9, 177.2, 181.5	99.5, 99.1, 108.7
α, β, γ (°)	90.0, 90.0, 90.0	90.0, 90.0, 90.0	92.6, 96.2, 120.1
Molecules in AU[a]	2	6	6
Wavelength	1.11587	1.11587	1.11587
Resolution range (Å)	1.80–78.50	2.92–127.13	2.93–107.35
Highest shell (Å)	1.80–1.85	2.92–3.00	2.93–3.01
Unique reflections	115,584 (7204)[b]	83,269 (6049)	74,605 (5556)
R_{sym} or R_{merge} (%)	5.9 (286.0)	40.0 (469.4)	19.3 (342.7)
$I/\sigma I$	17.7 (0.5)	7.1 (0.6)	5.3 (0.3)
Completeness (%)	98.2 (83.9)	100.0 (99.9)	97.9 (97.9)
Redundancy	11.4 (5.4)	13.5 (13.6)	3.4 (3.5)
Crystallization conditions	15% PEG[c] 3350, 200 mM sodium-malate, pH 6.8–7.2	0.1 M Na-cacodylate, 2% Jeffamine M-600, pH 7.0; 0.12 M guanidinium chloride	0.1 M sodium citrate, pH 5.6; 12% PEG 3350
Refinement statistics			
No. reflections	109,450	79,148	67,944
R_{work}/R_{free} (%)	18.5/22.7 (45.9/45.8)	20.9/29.1 (38.9/38.8)	21.4/30.8 (42.2/49.0)
No. atoms			
Protein	7184	21,135	19,552
Heme	172	258	258
Inhibitor	None	150	186
Solvent	510	46	1
Wilson plot B[d]	44.6	70.6	83.1
Mean B value	49.7	79.0	98.9
B factors			
Protein	50.2	81.0	101.9
Heme	35.5	60.6	67.1
Inhibitor	N/A[e]	70.2	79.5
Solvent	54.0	45.6	41.4
R.m.s[f] deviations			
Bond lengths (Å)	0.019	0.011	0.012
Bond angles (°)	1.974	1.577	1.643
Ramachandran statistics			
Preferred (%)	97.14	88.25	83.76
Allowed (%)	2.29	7.48	10.25
Outliers (%)	0.57	4.26	5.99

[a]Asymmetric unit
[b]Data for the highest resolution shell are shown in parentheses.
[c]Polyethylene glycol
[d]Temperature factor
[e]Not applicable
[f]Root-mean-square

was constructed using CHARMM-GUI (Jo et al., 2008). The simulation was conducted in a box containing protein, lipid membrane, water molecules, and ions. The AMBER14SB (Maier et al., 2015) and LIPID17 (Case et al., 2018) force fields were used for protein and lipids, respectively, whereas the heme group parameters were taken from Rydberg et al. (2007). Protonation states of the amino acid residues were determined at physiologic pH (pH = 7.14) using the PDB2PQR server (Dolinsky et al., 2004). Systems setup was performed with tleap program of Amber18 (Case et al., 2018). The system was solvated with explicit transferable intermolecular potential with 3 points (TIP3P) water molecules (Jorgensen and Jenson, 1998) in a cubic box extending at least 10 Å from the solute surface treated with periodic boundary conditions. Net charges were neutralized by replacing water molecules with Na^+ and Cl^- ions.

All MD simulations were conducted using NAMD v.2.13 program (Phillips et al., 2005). The 50,000 steps of energy minimization were performed to eliminate the atomic clashes. The lipid bilayer equilibration procedure was performed at constant pressure (1 atm) and constant temperature (298 K), for 150 nanoseconds with 1 $kcal \cdot mol^{-1} \cdot Å^{-2}$ harmonic position restraints applied to the protein backbone and heme. Further equilibration of the systems was performed at 1 atm and 298 K for 15 nanoseconds with all atoms unrestrained. Conventional MD simulation was performed for 250 nanoseconds at 1 atm and 298 K with a constant ratio constraint applied to the lipid bilayer in the X-Y plane.

Results

Oligomerization of AcCYP51 in Solution. An expression construct of AcCYP51 lacking the transmembrane helix and containing an exogenous 10–amino acid lead sequence at the N terminus and a hexahistidine tag at the C terminus was synthesized (Supplemental Data 1). Four chromatographic steps were used to purify AcCYP51: affinity chromatography on Ni-NTA resin, ion-exchange chromatography on Q Sepharose, hydroxyapatite chromatography, and, finally, size-exclusion chromatography on Superdex 200 XK 26 coupled to multi-angle light scattering (SEC-MALS).

On the size-exclusion column, AcCYP51 migrated in two peaks corresponding to molecular masses (MMs) of 100.0 ± 0.1 kDa (major peak, P1) and 57.40 ± 0.06 kDa (minor peak, P2) according to a calibration curve (R^2 = 0.9999) built using commercial MM markers (catalog 1511901; Bio-Rad Laboratories, Hercules, CA) (Fig. 1, A and B). The absolute MM

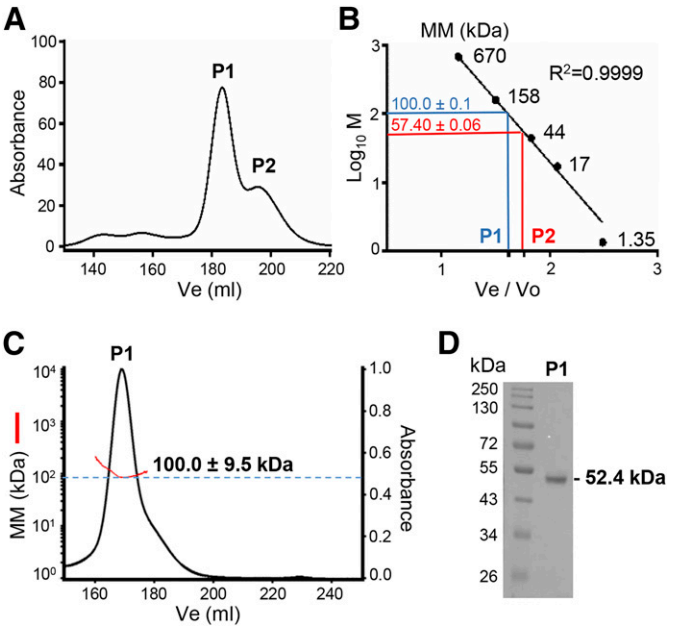

Fig. 1. Size-exclusion chromatography and SDS-PAGE of recombinant AcCYP51. (A) Size-exclusion chromatography profile of the heterogenous mixture of recombinant AcCYP51 on the Superdex 200 XK 26 column. (B) Molecular mass (MM) estimation of the P1 and P2 fractions. *y*-Axis represents log of MM in kilodaltons; *x*-axis represents ratio of elution volume (Ve) and void volume (Vo). Black dots (•) represent MM of the gel-filtration standards from the commercial calibration kit. Blue and red lines orthogonal to the axes correspond to different AcCYP51 populations: P1 with MM of 100.0 kDa and P2 with MM of 57.4 kDa. (C) SEC-MALS analysis of P1 peak showing experimental MM of the P1 fraction of 100.0 kDa (red line). (D) SDS-PAGE analysis of the purified P1 fraction.

of the P1 fraction determined by MALS constituted 100.0 ± 9.5 kDa (Fig. 1C). On SDS-PAGE, P1 migrated consistent with the MM calculated for one polypeptide chain (52.4 kDa) (Fig. 1D). These data demonstrated that 1) AcCYP51 forms a dimer in solution and 2) the dimer is stable enough to undergo size-exclusion chromatography. We have not observed any higher oligomers, suggesting that the highest oligomeric state of AcCYP51 in solution was a dimer.

UV-Visible Spectroscopic Properties of Recombinant AcCYP51. The dimeric and monomeric protein fractions separated by size-exclusion chromatography were individually analyzed by UV-visible spectroscopy (Fig. 2). The ferric AcCYP51 dimer, P1 fraction, had a typical CYP spectrum with the absorbance maxima at 418 nm and the ratio of absorbance at λ_{max} of the Soret band, 418 nm, to that at 280 nm of 1.8 to 1.9 (Fig. 2A, solid line). The ferrous-CO complex of the dimeric AcCYP51 had a high content of the P450 form (Fig. 2, A and B, dashed line). The monomeric AcCYP51, P2 fraction, was largely P420 (Fig. 2, C and D). A trace of P450 absorbance was likely due to residual contamination with the P1 fraction. To confirm that the AcCYP51 dimer in the crystals remained in the P450 form, we harvested the crystals, dissolved them in assay buffer, and recorded the UV-visible difference spectra. Upon sodium dithionite reduction and carbon monoxide binding, peak at 448 nm was observed (Fig. 2, E and F).

Overall X-Ray Structure of the AcCYP51 Dimer. The dimeric AcCYP51 readily crystallized in the absence of added ligands. The crystal structure at 1.8 Å revealed a symmetrical head-to-head homodimer with swapped N termini (Fig. 3A). The first seven amino acids of the lead sequence were disordered and not visible in electron density. The next three exogenous residues from the lead sequence (K40-G41-K42, yellow in Fig. 3B) followed by authentic AcCYP51 sequence participated in the N-terminal swapping. As shown in Fig. 3B, only the main chain of the K40-G41-K42 fragment participates in intermolecular protein-protein interactions, whereas the lysine side chains face the bulk solvent.

The overall protein scaffold was similar to that of monomeric CYP enzymes with the qualification that the region of K40-P52 containing the first strand of the β-sheet-1 (β1-1) was swapped between the two protomers and was parallel to the β1-2 of the interacting protomer instead of folding with the own polypeptide chain (Fig. 3A). Because of the swap, the A′ helix (F53-G63) established close intramolecular contacts with the F′ helix, blocking access to the active site. This block of access to the active site was reinforced by the intermolecular contacts in the dimer interface where the protomers faced each other through the A′, F′, F, and G α-helices (Fig. 3A). A dimer protein-protein interface of 2000 Å^2 was calculated using the Protein Interfaces, Surfaces, and Assemblies software (Krissinel and Henrick, 2007). Altogether, 16 H-bonds and two salt bridges stabilized the protein-protein interface formed by 40 hydrophobic residues provided by each protomer. The buried surface constituted 10% of the accessible surface of AcCYP51 and provided total solvation energy gain of −35.4 kcal/mol. F84 had the most prominent single residue input of −2.1 kcal/mol (Fig. 3C). This protein-protein interface was strong enough to sustain size-exclusion chromatography and crystallization in up to 1 M urea. Crystals obtained in 0.55 M urea diffracted to 1.85 Å and had intact dimeric structure similar to that seen in native conditions.

Heme Binding. An unusual feature of the AcCYP51 dimer was heme "wobbling." Despite the multiple H-bonding interactions with Y114, Y127, and Q110 and a salt bridge with R368 formed by the heme propionate moieties, two alternative conformations were required to approximate the heme position in the ligand-free AcCYP51 (Fig. 3D). In heme conformers, the Fe-S bond length was refined between 2.33 and 2.41 Å. The 2.41-Å bond length goes beyond the range reported for other crystallographically resolved P450 enzymes (Lewis et al., 2006). Consistent with the ferric resting state, the water molecule was modeled in both protomers as a sixth, axial iron ligand at the distances of ≤2.64 Å of the heme iron (Fig. 3D).

Overall X-Ray Structures of the Inhibitor-Bound AcCYP51. AcCYP51 cocrystallized with clotrimazole or isavuconazole as a monomer; crystals diffracted to a resolution of 2.9 Å. In both structures, the asymmetric unit contained six inhibitor-bound AcCYP51 molecules. In each molecule, electron density for the bound inhibitor was unambiguously defined as evidenced by the omit maps in Fig. 4, A and B. In clotrimazole-bound AcCYP51, the β1-1 region folded back to its own polypeptide chain, restoring a typical P450 scaffold. Two consecutive glycine residues in the A-A′ loop, G^{62}-G^{63}, served as a hinge facilitating swinging of the upstream part (Fig. 4, C and D). In a remarkable contrast to clotrimazole, 74 N-terminal residues were disordered and missing from the electron density of the AcCYP51-isavuconazole complex (Fig. 4E). From the comparison of three structures (Fig. 4, C–E), the β1-1 strand and the A′, B′, and F′ helices progressively loose the canonical H-bonding patterns from ligand-free dimer to clotrimazole complex to isavuconazole complex. In the

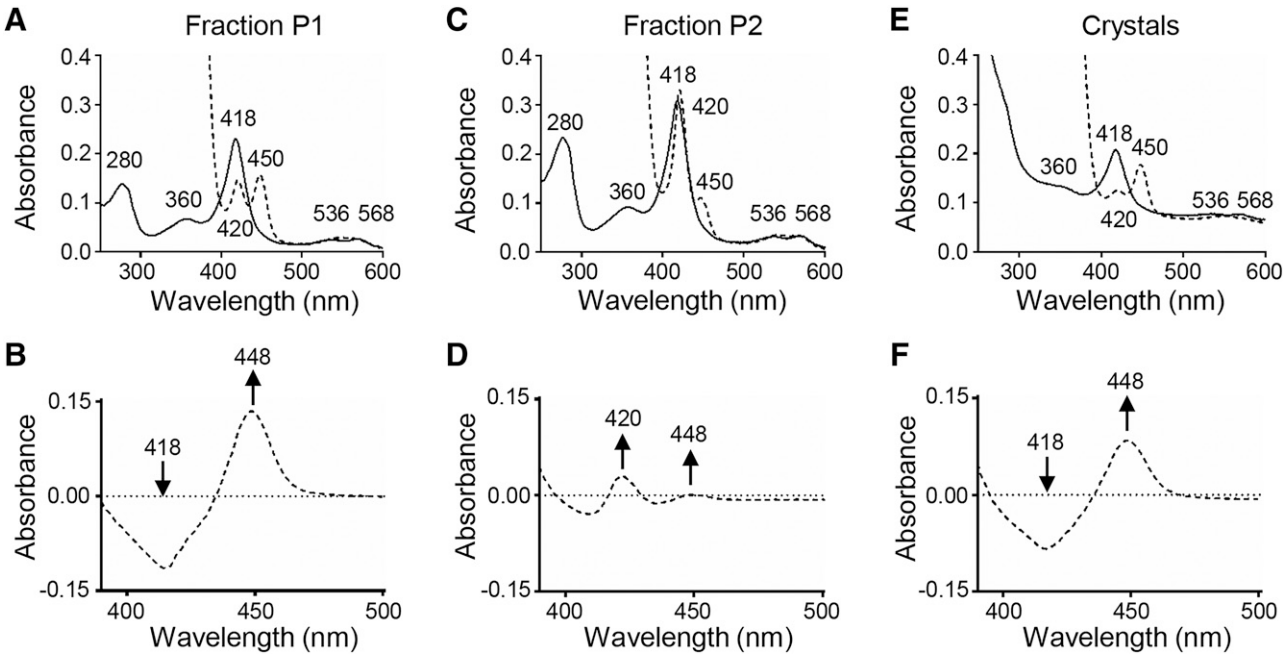

Fig. 2. UV-visible spectroscopy analysis of AcCYP51. (A) Absolute UV-visible spectra of the purified P1 fraction of AcCYP51 showing characteristic peaks at 280, 360, 418, 536, and 568 nm; ferric Fe^{3+}, solid line. Sodium dithionite–reduced CO-bound ferrous-Fe^{2+} form shows peaks at 420 and 450 nm, dashed line. (B) CO-bound difference spectra of the sodium dithionite–reduced dimeric fraction, P1. (C) Absolute spectra of the monomeric fraction, P2; ferric Fe^{3+}, solid line; CO-bubbled sodium dithionite–reduced ferrous Fe^{2+}, dashed line. (D) CO-bound difference spectra of the sodium dithionite–reduced monomeric fraction, P2. (E) Absolute spectra of the AcCYP51 recovered from the dimer crystals; ferric Fe^{3+}, solid line; CO-bubbled sodium dithionite–reduced ferrous Fe^{2+}, dashed line. High absorbance <300 nm is an artifact of measurements in plastic cuvette. (F) CO-bound difference spectra of the sodium dithionite–reduced AcCYP51 recovered from the dimer crystals.

AcCYP51-isavuconazole structure, the β1-1, A′, and A atomic coordinates are not included.

AcCYP51-Clotrimazole Complex in the Crystal. The structure determined in this work is the first of the CYP51-clotrimazole complex. Similar to other P450-clotrimazole structures [CYP46A1 (PDB ID: 3MDV), P450 BM3 (6H1T), EryK (2XFH), and OleP (4XE3)], clotrimazole bound in the active site of AcCYP51 via a coordination bond provided to the heme iron by the aromatic nitrogen of the imidazole moiety and via the hydrophobic interactions mediated by the phenyl moieties of the drug. The orientation of the chlorophenyl moiety in clotrimazole varies between different CYP enzymes. In AcCYP51, the short side chain of S117 defines orientation of the chlorophenyl moiety by providing space to accommodate a bulky Cl substituent that is within 5.1 Å of the serine carboxyl group (Fig. 4A). Other contacts within 5 Å of clotrimazole involve Y114, F116, S117, F121, V126, T127, L216, A290, F293, A294, H297, L363, and V366. Compared with the inhibitor-free AcCYP51, the first-tier residues in the substrate-binding site are shifted away from clotrimazole to accommodate the inhibitor. To compensate for the inhibitor-introduced distortions, this trend was propagated to the second and third tier residues. From the perspective of drug design, the tight fit in the active site leaves room for derivatization of only one phenyl moiety in clotrimazole.

AcCYP51-Isavuconazole Complex in the Crystal. The structure determined in this work is the first of the P450-isavuconazole complex. Similar to clotrimazole, isavuconazole bound in the heme pocket via coordination to the heme iron and protein-drug interactions (Fig. 4B). In the heme pocket, the set of interacting residues is similar to that of clotrimazole excluding L216 and H297. More-elongated isavuconazole molecule also makes interactions with F365, M367, and M471 with the thiazolyl benzonitrile moiety of the drug. The nitrile group points toward the opening created by disordering of the A′ and F′ helices.

Stability of the AcCYP51-Ligand Complexes in Solution. The binding of the inhibitors and substrates was assessed by the shift of the Fe Soret band in the UV-visible spectra of dimeric AcCYP51 (Fig. 5). Type II binding spectra were obtained upon clotrimazole and isavuconazole binding (Fig. 5A). Type I spectra were obtained upon binding sterols lanosterol and 31-norlanosterol, with qualification that 31-norlanosterol generated a larger spectral response than lanosterol (Fig. 5B). Binding kinetics of AcCYP51 at saturating ligand concentrations showed that both isavuconazole and clotrimazole reached saturation for <10 minutes, whereas more than 30 minutes were required for 31-norlanosterol to reach the saturation (Fig. 5, C and D). Magnitude of the spectral changes suggested that only 10%–20% of AcCYP51 resulted in the formation of enzyme-ligand complexes (Table 2).

When AcCYP51 was titrated with clotrimazole, a typical binding curve was obtained, and K_D of 152.3 ± 10.0 nM was calculated by fitting binding data using the Morrison "quadratic" equation (Morrison, 1969) (Fig. 5E). For isavuconazole, the binding plateau could not be reached (Fig. 5E). In the context of our structural data, isavuconazole may have affected integrity of AcCYP51 and the magnitude of the Soret spectral shift by partial protein unfolding.

Modeling AcCYP51 Dimer Interactions with the ER Membrane. To assess compatibility of the domain-swap dimerization with membrane binding, we built a molecular

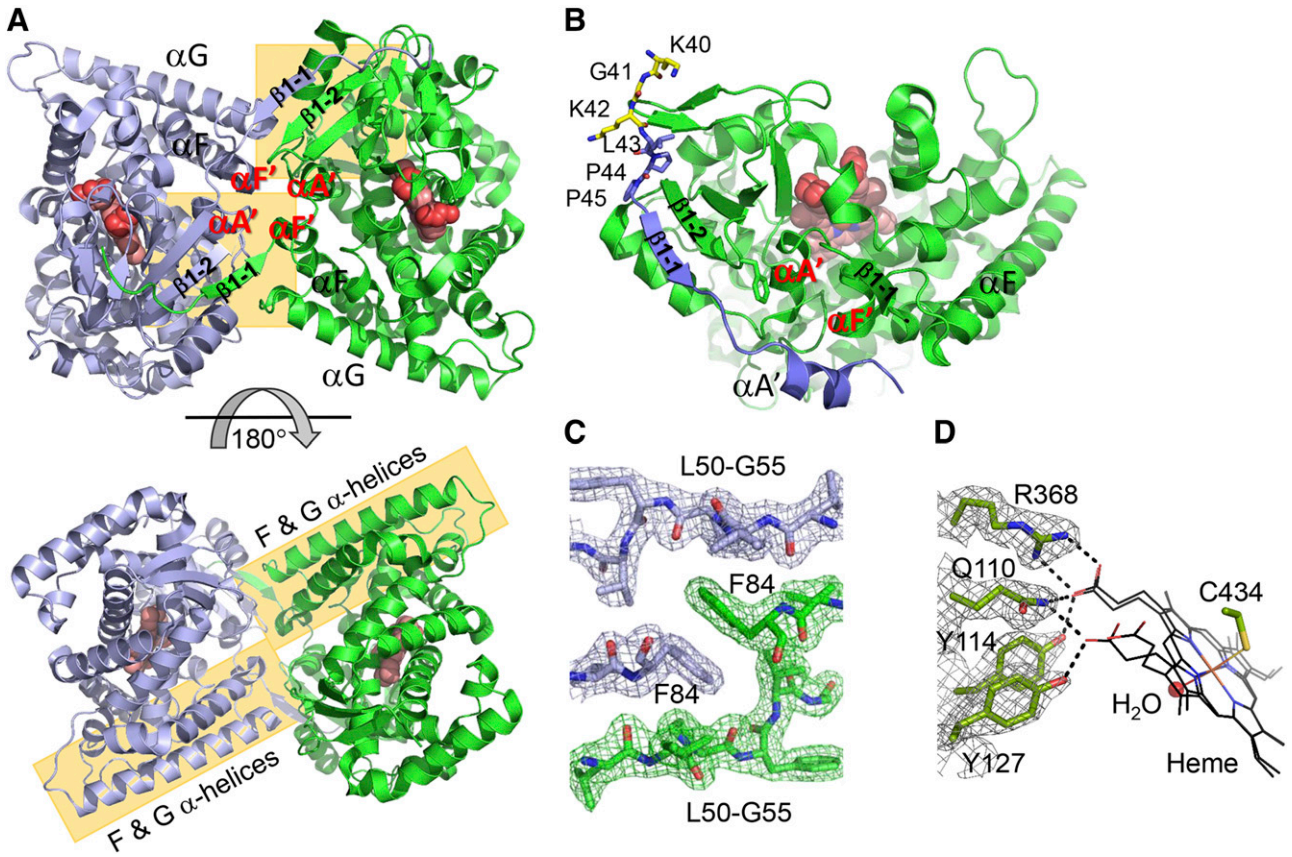

Fig. 3. X-ray structure of the AcCYP51 dimer. (A) Head-to-head dimer is shown in ribbon representation. The protomers are in blue and green. The heme prosthetic group is in pink Van der Waals spheres; oxygen atoms of the heme propionate moieties are in red. Interfacing secondary structure elements are shaded in yellow. (B) Interactions of the swapped fragment (blue) with adjacent protomer (green). A fragment of the exogenous leading sequence is shown in yellow. Authentic AcCYP51 sequence is in blue. (C) A fragment of the $2F_o$-F_c electron density map contoured at 1.2 σ (blue and green mesh) shows interactions of F84, a residue at the dimer interface with the most prominent solvation energy gain. (D) Heme in two alternative conformations is shown in black lines. Heme propionate groups interactions with the amino acid residues within 3.2 Å are indicated by the dashed lines. Coordination bonds to the heme axial ligands C434 and water molecule (red sphere) are shown.

model of AcCYP51-membrane interactions. The wild-type N-terminal residues omitted from the recombinant AcCYP51 were added computationally. The fully reconstructed AcCYP51 dimer was embedded into a lipid membrane constituted of phospholipids, POPC/POPE, and cholesterol found in the membranes of higher eukaryotes. Cholesterol was used in MD simulations to optimize conformation of the TM helix (residues 10–30) and its flanking regions because the Amber force field does not have the parameter for ergosterol found in the membranes of lower eukaryotes.

The model demonstrated that the dimerization mode observed in the crystal structure is compatible with the membrane association (Fig. 6A). The TM helices are separated in space and run virtually orthogonal to the lipid bilayer, which is consistent with the relatively short TM helix in AcCYP51. The region connecting the TM helix with the globular CYP domain is predicted to be a flexible loop up to the downstream segment 44–51, which adopts a β-strand structure (β1-1) running parallel to β1-2 of the interacting protomer.

In addition to the TM helix, protein-lipid interactions occur through the regions corresponding to residues 31–43 (Fig. 6B). This fragment has several charged amino acids (i.e., K31, R33, E34, R36 and K37), which interact with the zwitterionic heads of POPC and POPE phospholipids. On the other hand, the presence of hydrophobic residues, such as V32 and L43, enables the nonpolar interactions between the linker regions and lipid tails (Fig. 6B). Finally, W35, Y38, and Y41 act as anchoring residues, which are usually located between the polar group and the hydrophobic core of the lipid bilayer in the glycerol region of the membrane (Mustafa et al., 2019).

The β5-β6 segment (residues 372–380) also faces the membrane in our model and is partially immersed in its hydrophobic environment. Finally, in one of the monomers, residues R273, G274, and E275 tend to associate with lipid heads (Fig. 6B). The electrostatic potential density at the surface of AcCYP51 dimer shows that the membrane-associated protein surface comprises charged patches, thus supporting the reliability of our membrane-insertion model (Fig. 6C).

Discussion

CYP enzymes are a superfamily of *b*-type heme-containing monooxygenases descended from a single common ancestor (Gotoh, 2012). They share structural features, such as a common protein scaffold, the similarity in positioning of the heme group, and the access/egress pathways for substrates and products (Otyepka et al., 2007). The heme group is bound via a thiolate sulfur bond donated by the universally conserved "proximal" cysteine residue at the fifth, axial coordination of the heme iron. The heme iron binds molecular oxygen, O_2, as

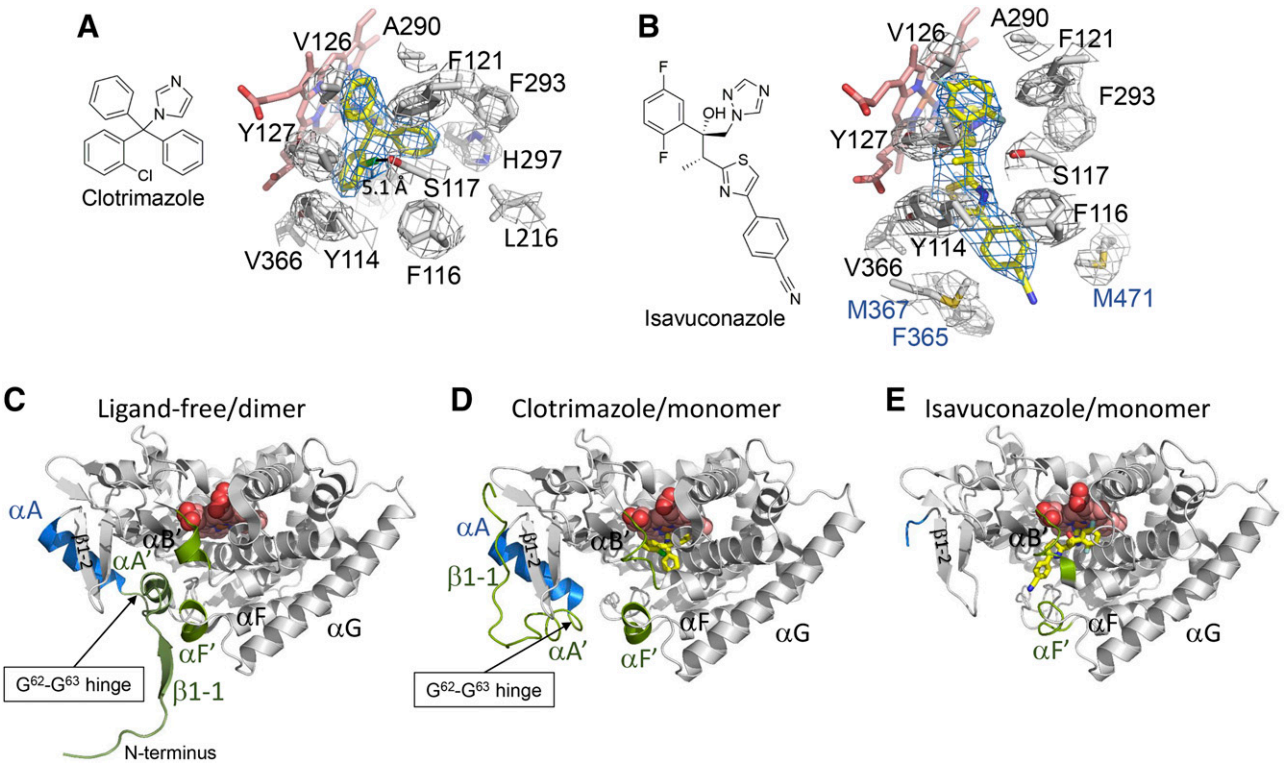

Fig. 4. AcCYP51-inhibitor complexes. (A) Clotrimazole bound in the active site. (B) Isavuconazole bound in the active site. In (A and B), inhibitors are shown in yellow, heme is shown in pink, and amino acid side chains within 5 Å are shown in gray. The fragments of the $2F_o$-F_c electron density omit map (blue and gray mesh) are countered at 1.0 σ. Chemical structures of the inhibitors are shown as two-dimensional diagrams. (C–E) Ribbon representations of the superimposed AcCYP51 from the inhibitor-free (dimeric) and inhibitor-bound (monomeric) structures. The equivalent positions corresponding to the N terminus, the β1-1 strand, the A′, B′, and F′ helices are colored in green and to the αA helix in blue. Heme is in pink Van der Waals spheres; clotrimazole and isavuconazole are yellow in stick mode. Nitrogen atoms are in blue, oxygen in red, chlorine in green, and fluorine in cyan.

a sixth ligand in the "distal" pocket, which also serves as a site for substrate binding. CO resembles O_2 in size and heme-binding properties. By replacing O_2, CO blocks the enzymatic turnover of the CYP enzymes. CO is used as a sensitive probe of local conformation and dynamics in the active site of heme-thiolate proteins. Absorption spectra of the CO-bound ferrous CYP enzymes (Fe^{2+}–CO) often display two Soret bands in the blue region of the visible range, which are denoted P420 and P450. The 420- and 450-nm bands are arguably assigned to CYP species having, respectively, a protonated (thiol) and deprotonated (thiolate) cysteine side chain as axial iron ligands (Perera et al., 2003; Dunford et al., 2007; Sabat et al., 2009; Driscoll et al., 2011). Alternatively, recruitment of a histidine residue to replace the native cysteine thiolate ligand has been suggested (Martinis et al., 1996; Sun et al., 2013). Finally, theoretical calculations indicate that stretching the Fe-S bond by only 0.2 Å could induce the spectral transition of ferrous CO P450 to P420 (Jung et al., 1979). A variety of extreme conditions, such as heating, hydrostatic pressure, organic solvents, and denaturants, were used to convert P450 to P420 (Martinis et al., 1996; Sun et al., 2010; Arendse and Blackburn, 2018; Chen et al., 2019). On a few occasions, P420 could be converted back to P450 (Ogura et al., 2004; Dunford et al., 2007).

The mechanistic knowledge accumulated in the field supports the assumption that a CYP monomer is sufficient for catalytic function, and CYP dimerization is not required for the act of catalysis. At the same time, there are reports of CYP-CYP interactions both in microsomal membranes (Greinert et al., 1982; Kawato et al., 1982; Myasoedova and Berndt, 1990; Schwarz et al., 1990; Myasoedova and Magretova, 2001; Szczesna-Skorupa et al., 2003; Ozalp et al., 2005; Praporski et al., 2009; Hu et al., 2010; Davydov et al., 2015) and in recombinant CYP proteins (Myasoedova and Berndt, 1990; Von Wachenfeldt and Johnson, 1995; Von Wachenfeldt et al., 1997; Davydov et al., 2005, 2010, 2013; Reed et al., 2012). CYP-CYP interactions are suggested to play regulatory rather than catalytic role (Reed and Backes, 2017). Despite biophysical and biochemical evidence, details of CYP-CYP interaction mode(s) remain obscure. The protein-protein interfaces reported in the crystal structures of the multimolecular complexes of eukaryotic CYP enzymes are random and have small interaction areas (Reed and Backes, 2017). These considerations encouraged us to determine the first X-ray structure of a sustainable CYP51 dimer. This in turn led to discovery of the domain-swap dimerization mode.

The P450 character of the AcCYP51 dimer contrasts with the P420 character of the AcCYP51 monomer. The propensity of AcCYP51 to convert into a P420 form even in mild purification conditions was consistent with the flexibility of the heme pocket manifested by heme wobbling and lengthening of the Fe-S bond as observed in the crystal structure. We speculate that dimerization in AcCYP51 plays a stabilizing role to maintain the functional status of the heme.

The modifications introduced at the N terminus of AcCYP51 to enable expression in the bacterial host may potentially

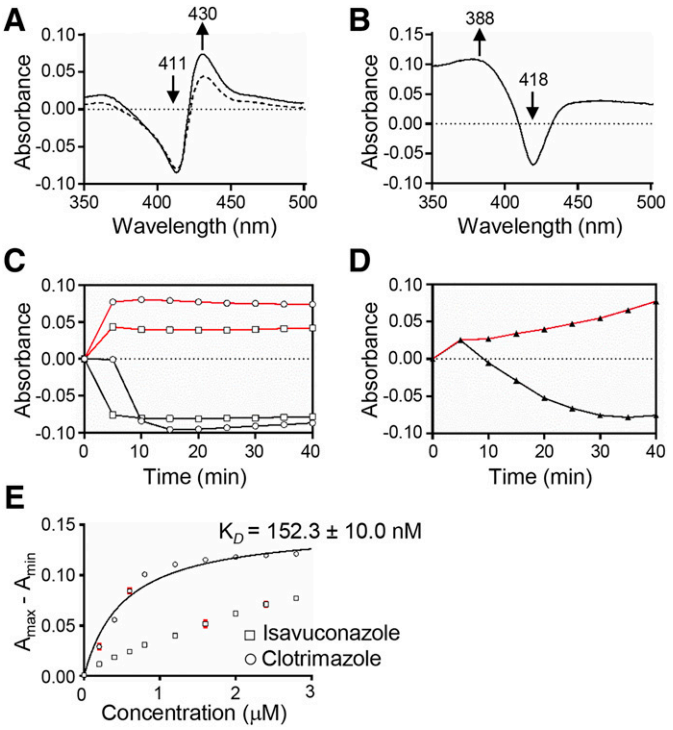

Fig. 5. Ligand-binding properties of the AcCYP51 dimer. (A) Type II difference binding spectra of 20 μM isavuconazole (dashed line) and 20 μM clotrimazole (solid line) to 5 μM AcCYP51. (B) Type I difference binding spectra of 20 μM 31-norlanosterol to 5 μM AcCYP51. (C) Binding kinetics of 20 μM isavuconazole (open squares) and clotrimazole (open circles) to 5 μM AcCYP51 at 430 (red curves) and 411 nm (black curves). (D) Binding kinetics of 20 μM 31-norlanosterol to 5 μM AcCYP51 at 388 (red curve) and 418 nm (black curve). Experiments in (C and D) were performed twice. A representative time course is shown for each ligand. Percentage of the ligand-bound fraction in Table 2 is calculated based on duplicates. (E) Binding isotherms of isavuconazole and clotrimazole; A_{max} is absorbance at 430, and A_{min} is absorbance at 410 nm. AcCYP51 concentration is 1 μM. S.D. are shown in red. For most data points, deviations are smaller than the size of the symbols.

affect the behavior of the recombinant protein. However, truncation of the TM helix and insertion of an exogenous lead sequence is a commonly used practice to express microsomal CYP enzymes, but CYP dimerization via N-termini swap has not been reported. Furthermore, exogenous residues in the lead sequence are not involved in the dimer interface, making N-termini swapping an interesting paradigm of CYP dimerization.

The interactions between CYP enzymes and cell membranes are crucial for establishing protein orientation in the membrane, which is described as a dynamic process (Šrejber et al., 2018). The membrane positioning is recognized as an essential factor facilitating substrate/product channeling to the active site and interactions with the redox partners (Šrejber et al., 2018). Our modeling studies demonstrated that N-termini swap dimerization is compatible with membrane topology both spatially and electronically. It also does not contradict experimental data obtained elsewhere by different biophysical and biochemical methods. A model of the *Saccharomyces cerevisiae* CYP51 monomer embedded in phospholipid bilayer serves as a current paradigm of CYP-membrane interactions (Monk et al., 2014). The F-G loop region involved in protein-protein interactions in AcCYP51 dimer is predicted to be embedded in the lipid bilayer in *S. cerevisiae* CYP51 (Monk et al., 2014). Hypothetically, transition between the two membrane-association modes would depend on the flexibility of the hinge region (two consecutive glycine residues, G^{62}-G^{63}, in the A-A′ loop of AcCYP51). A flexible hinge would facilitate dissociation of globular domain from the lipid bilayer and association into a homodimer.

We inspected the glycine-rich and highly variable A-A′ loop in human CYP enzymes. Two consecutive glycine residues are especially prominent in human CYP46A. This is an important central nervous system enzyme that converts cholesterol to 24S-hydroxycholesterol, thereby initiating the major pathway of cholesterol removal from the brain (Björkhem et al., 1997). Multiple X-ray structures of CYP46A1 in complex with a variety of drugs (antidepressants, anticonvulsants, and antifungals) are available in the PDB. Remarkably, in all these entries, CYP46A1 is missing 50 N-terminal residues and is therefore truncated shortly upstream of the G-G motif. This observation supports our hypothesis that the CYP globular domain may be loosely associated with the N terminus and has freedom to dimerize on the membrane surface.

Based on the structural insights obtained from AcCYP51 alone and the AcCYP51-inhibitor complexes, the superior potency of isavuconazole against *A. castellanii* may be explained by partial denaturing of the AcCYP51 target. Given that access to the AcCYP51 active site is blocked by dimerization, to bind an inhibitor or substrate the dimer has to dissociate. This assumption is consistent with the slow rate of ligand binding (10 minutes for clotrimazole and isavuconazole and 30 minutes for 31-norlanosterol), low drug-target complex fraction (10%–20%), and the monomeric form of the AcCYP51-clotrimazole and AcCYP51-isavuconazole complexes observed in the crystals. Partial denaturing of AcCYP51 in response to inhibitor binding (74 disordered N-terminal residues in the AcCYP51-isavuconazole complex) suggests a mechanism of action fundamentally different from conventional enzyme inhibition by blocking the active site. In living cells, structurally aberrant AcCYP51 may undergo further denaturation and be permanently deactivated by proteolytic degradation. In the context of the superior activity of isavuconazole, this

TABLE 2
UV-visible quantification of the AcCYP51 ligand-bound fraction[a]

Ligand	Ligand, μM	AcCYP51, μM	AcCYP51 ligand, μM		Fraction of ligand-bound AcCYP51, %	
			*n*1	*n*2	*n*1	*n*2
Clotrimazole	20.0	5.0	0.81	0.66	16.2	13.0
Isavuconazole	20.0	5.0	0.47	0.38	9.4	7.6
31-Norlanosterol	20.0	5.0	0.90	1.00	18.0	20.0

[a]Experiments were performed in duplicates. Values for the replicates *n*1 and *n*2 are shown separately.

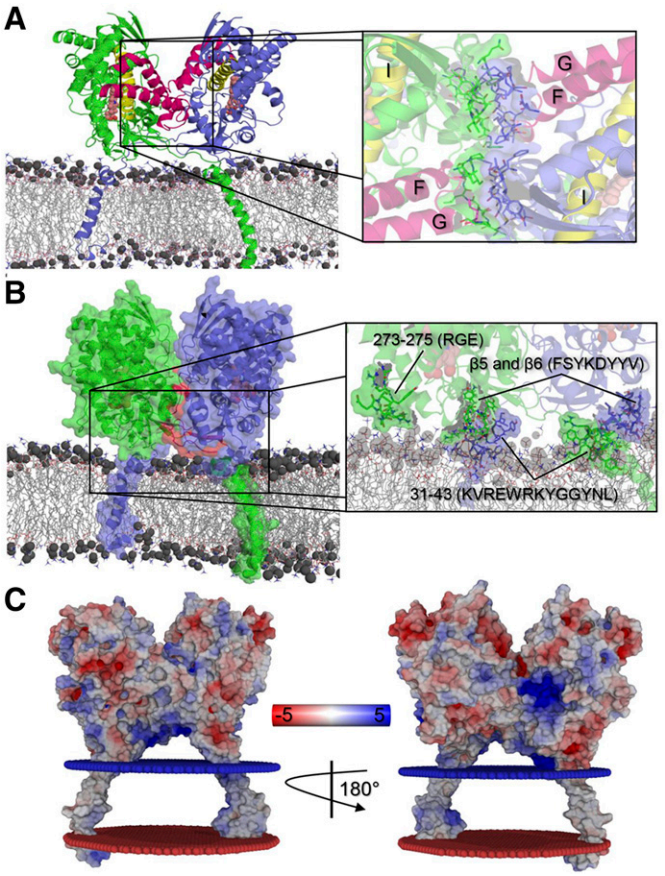

Fig. 6. Molecular model of the AcCYP51 dimer in a phospholipid bilayer. (A) The full-length AcCYP51 dimer with the reconstituted TM helix is colored in blue and green. The F and G helices are highlighted in magenta, the I helix is in yellow, and heme is in pink Van der Waals spheres. Membrane lipids are in gray lines; phosphorous atoms of phospholipids are in black spheres. The dimer interface is displayed in the right panel, wherein the main interacting residues are depicted as sticks and surfaces. (B) Semitransparent surface representation of AcCYP51 dimer and a zoom in on protein-lipid interactions outside of the TM helices. The right panel zooms in on the protein-lipid interactions. The participating residues are labeled. (C) Electrostatic potential surface calculated for AcCYP51 dimer. The blue bead layer indicates the cytoplasmic side, and the red bead layer indicates the luminal side of the ER membrane.

phenomenon can be exploited for designing other AcCYP51 inhibitors that target the dimerization interface.

Acknowledgments

We thank Michael K. Gilson and Jeffry Setiadi, Skaggs School of Pharmacy and Pharmaceutical Sciences University of California San Diego (SSPPS-UCSD), for providing access to the computational resources; James McKerrow for valuable discussions and support of this project; and the Advanced Light Source (ALS) beamline 8.3.1 personnel James Holton, George Meigs, and Jane Tanamachi for assistance with the data collection.

Authorship Contributions

Participated in research design: Sharma, Hernandez-Alvarez, Podust.

Conducted experiments: Sharma, Shing.

Contributed new reagents or analytic tools: Hernandez-Alvarez.

Performed data analysis: Sharma, Shing, Debnath, Podust.

Wrote or contributed to the writing of the manuscript: Sharma, Hernandez-Alvarez, Podust.

References

Arendse LB and Blackburn JM (2018) Effects of polymorphic variation on the thermostability of heterogenous populations of CYP3A4 and CYP2C9 enzymes in solution. *Sci Rep* **8**:11876.

Björkhem I, Lütjohann D, Breuer O, Sakinis A, and Wennmalm A (1997) Importance of a novel oxidative mechanism for elimination of brain cholesterol. Turnover of cholesterol and 24(S)-hydroxycholesterol in rat brain as measured with 18O2 techniques *in vivo* and *in vitro*. *J Biol Chem* **272**:30178–30184.

Calvet CM, Vieira DF, Choi JY, Kellar D, Cameron MD, Siqueira-Neto JL, Gut J, Johnston JB, Lin L, Khan S, et al. (2014) 4-Aminopyridyl-based CYP51 inhibitors as anti-*Trypanosoma cruzi* drug leads with improved pharmacokinetic profile and *in vivo* potency. *J Med Chem* **57**:6989–7005.

Case DA, Ben-Shalom IY, Brozell SR, Cerutti DS, Cheatham TE III, Cruzeiro VWD, Darden TA, Duke RE, Ghoreishi D, Gilson MK, et al. (2018) *AMBER 2018*, University of California, San Francisco, CA.

Chen YJ, Zhang J, Zhu PP, Tan XW, Lin QH, Wang WX, Yin SS, Gao LZ, Su MM, Liu CX, et al. (2019) Stereoselective oxidation kinetics of deoxycholate in recombinant and microsomal CYP3A enzymes: deoxycholate 19-hydroxylation is an *in vitro* marker of CYP3A7 activity. *Drug Metab Dispos* **47**:574–581.

Choi JY, Calvet CM, Gunatilleke SS, Ruiz C, Cameron MD, McKerrow JH, Podust LM, and Roush WR (2013) Rational development of 4-aminopyridyl-based inhibitors targeting *Trypanosoma cruzi* CYP51 as anti-chagas agents. *J Med Chem* **56**: 7651–7668.

Choi JY, Calvet CM, Vieira DF, Gunatilleke SS, Cameron MD, McKerrow JH, Podust LM, and Roush WR (2014a) R-Configuration of 4-aminopyridyl-based inhibitors of CYP51 confers superior efficacy against *Trypanosoma cruzi*. *ACS Med Chem Lett* **5**:434–439.

Choi JY, Podust LM, and Roush WR (2014b) Drug strategies targeting CYP51 in neglected tropical diseases. *Chem Rev* **114**:11242–11271.

Collaborative Computational Project, Number 4 (1994) The CCP4 suite: programs for protein crystallography. *Acta Crystallogr D Biol Crystallogr* **50**:760–763.

Davydov DR, Davydova NY, Sineva EV, and Halpert JR (2015) Interactions among cytochromes P450 in microsomal membranes: oligomerization of cytochromes P450 3A4, 3A5, and 2E1 and its functional consequences. *J Biol Chem* **290**:3850–3864.

Davydov DR, Davydova NY, Sineva EV, Kufareva I, and Halpert JR (2013) Pivotal role of P450-P450 interactions in CYP3A4 allostery: the case of α-naphthoflavone. *Biochem J* **453**:219–230.

Davydov DR, Fernando H, Baas BJ, Sligar SG, and Halpert JR (2005) Kinetics of dithionite-dependent reduction of cytochrome P450 3A4: heterogeneity of the enzyme caused by its oligomerization. *Biochemistry* **44**:13902–13913.

Davydov DR, Sineva EV, Sistla S, Davydova NY, Frank DJ, Sligar SG, and Halpert JR (2010) Electron transfer in the complex of membrane-bound human cytochrome P450 3A4 with the flavin domain of P450BM-3: the effect of oligomerization of the heme protein and intermittent modulation of the spin equilibrium. *Biochim Biophys Acta* **1797**:378–390.

Debnath A, Calvet CM, Jennings G, Zhou W, Aksenov A, Luth MR, Abagyan R, Nes WD, McKerrow JH, and Podust LM (2017) CYP51 is an essential drug target for the treatment of primary amoebic meningoencephalitis (PAM). *PLoS Negl Trop Dis* **11**:e0006104.

Dolinsky TJ, Nielsen JE, McCammon JA, and Baker NA (2004) PDB2PQR: an automated pipeline for the setup of Poisson-Boltzmann electrostatics calculations. *Nucleic Acids Res* **32**:W665–W667.

Driscoll MD, McLean KJ, Cheesman MR, Jowitt TA, Howard M, Carroll P, Parish T, and Munro AW (2011) Expression and characterization of *Mycobacterium tuberculosis* CYP144: common themes and lessons learned in the *M. tuberculosis* P450 enzyme family. *Biochim Biophys Acta* **1814**:76–87.

Dunford AJ, McLean KJ, Sabri M, Seward HE, Heyes DJ, Scrutton NS, and Munro AW (2007) Rapid P450 heme iron reduction by laser photoexcitation of *Mycobacterium tuberculosis* CYP121 and CYP51B1. Analysis of CO complexation reactions and reversibility of the P450/P420 equilibrium. *J Biol Chem* **282**:24816–24824.

Emsley P and Cowtan K (2004) Coot: model-building tools for molecular graphics. *Acta Crystallogr D Biol Crystallogr* **60**:2126–2132.

Gotoh O (2012) Evolution of cytochrome p450 genes from the viewpoint of genome informatics. *Biol Pharm Bull* **35**:812–817.

Greinert R, Finch SA, and Stier A (1982) Cytochrome P-450 rotamers control mixed-function oxygenation in reconstituted membranes. Rotational diffusion studied by delayed fluorescence depolarization. *Xenobiotica* **12**:717–726.

Hu G, Johnson EF, and Kemper B (2010) CYP2C8 exists as a dimer in natural membranes. *Drug Metab Dispos* **38**:1976–1983.

Jo S, Kim T, Iyer VG, and Im W (2008) CHARMM-GUI: a web-based graphical user interface for CHARMM. *J Comput Chem* **29**:1859–1865.

Jorgensen WL and Jenson C (1998) Temperature dependence of TIP3P, SPC, and TIP4P water from NPT Monte Carlo simulations: seeking temperatures of maximum density. *J Comput Chem* **19**:1179–1186.

Jung C, Friedrich J, and Ristau O (1979) Quantum chemical interpretation of the spectral properties of the CO and O2 complexes of hemoglobin and cytochrome P-450. *Acta Biol Med Ger* **38**:363–377.

Kabsch W (2010) XDS. *Acta Crystallogr D Biol Crystallogr* **66**:125–132.

Kawato S, Gut J, Cherry RJ, Winterhalter KH, and Richter C (1982) Rotation of cytochrome P-450. I. Investigations of protein-protein interactions of cytochrome P-450 in phospholipid vesicles and liver microsomes. *J Biol Chem* **257**:7023–7029.

Koehler Leman J and Bonneau R (2018) A novel domain assembly routine for creating full-length models of membrane proteins from known domain structures. *Biochemistry* **57**:1939–1944.

Koehler Leman J, Mueller BK, and Gray JJ (2017) Expanding the toolkit for membrane protein modeling in Rosetta. *Bioinformatics* **33**:754–756.

Krissinel E and Henrick K (2007) Inference of macromolecular assemblies from crystalline state. *J Mol Biol* **372**:774–797.

Lamb DC, Warrilow AGS, Rolley NJ, Parker JE, Nes WD, Smith SN, Kelly DE, and Kelly SL (2015) Azole antifungal agents to treat the human pathogens

Acanthamoeba castellanii and *Acanthamoeba polyphaga* through inhibition of sterol 14α-demethylase (CYP51). *Antimicrob Agents Chemother* **59**:4707–4713.
Lewis DF, Ito Y, and Goldfarb PS (2006) Structural modelling of the human drug-metabolizing cytochromes P450. *Curr Med Chem* **13**:2645–2652.
Luthra A, Denisov IG, and Sligar SG (2011) Spectroscopic features of cytochrome P450 reaction intermediates. *Arch Biochem Biophys* **507**:26–35.
Maier JA, Martinez C, Kasavajhala K, Wickstrom L, Hauser KE, and Simmerling C (2015) ff14SB: improving the accuracy of protein side chain and backbone parameters from ff99SB. *J Chem Theory Comput* **11**:3696–3713.
Marciano-Cabral F and Cabral G (2003) *Acanthamoeba* spp. as agents of disease in humans. *Clin Microbiol Rev* **16**:273–307.
Martinis SA, Blanke SR, Hager LP, Sligar SG, Hoa GH, Rux JJ, and Dawson JH (1996) Probing the heme iron coordination structure of pressure-induced cytochrome P420cam. *Biochemistry* **35**:14530–14536.
Martín-Navarro CM, López-Arencibia A, Sifaoui I, Reyes-Batlle M, Valladares B, Martínez-Carretero E, Piñero JE, Maciver SK, and Lorenzo-Morales J (2015) Statins and voriconazole induce programmed cell death in *Acanthamoeba castellanii*. *Antimicrob Agents Chemother* **59**:2817–2824.
Monk BC, Tomasiak TM, Keniya MV, Huschmann FU, Tyndall JDA, O'Connell JD III, Cannon RD, McDonald JG, Rodriguez A, Finer-Moore JS, et al. (2014) Architecture of a single membrane spanning cytochrome P450 suggests constraints that orient the catalytic domain relative to a bilayer. *Proc Natl Acad Sci USA* **111**: 3865–3870.
Morrison JF (1969) Kinetics of the reversible inhibition of enzyme-catalysed reactions by tight-binding inhibitors. *Biochim Biophys Acta* **185**:269–286.
Mustafa G, Nandekar PP, Camp TJ, Bruce NJ, Gregory MC, Sligar SG, and Wade RC (2019) Influence of transmembrane helix mutations on cytochrome P450-membrane interactions and function. *Biophys J* **116**:419–432.
Myasoedova KN and Berndt P (1990) Cytochrome P-450LM2 oligomers in proteoliposomes. *FEBS Lett* **275**:235–238.
Myasoedova KN and Magretova NN (2001) Cross-Linking study of cytochrome P450 1A2 in proteoliposomes. *Biosci Rep* **21**:63–72.
Ogura H, Nishida CR, Hoch UR, Perera R, Dawson JH, and Ortiz de Montellano PR (2004) EpoK, a cytochrome P450 involved in biosynthesis of the anticancer agents epothilones A and B. Substrate-mediated rescue of a P450 enzyme. *Biochemistry* **43**:14712–14721.
Omura T and Sato R (1964) The carbon monoxide-binding pigment of liver microsomes. II. Solubilization, purification, and properties. *J Biol Chem* **239**:2379–2385.
Otyepka M, Skopalík J, Anzenbacherová E, and Anzenbacher P (2007) What common structural features and variations of mammalian P450s are known to date? *Biochim Biophys Acta* **1770**:376–389.
Ouellet H, Podust LM, and de Montellano PR (2008) *Mycobacterium tuberculosis* CYP130: crystal structure, biophysical characterization, and interactions with antifungal azole drugs. *J Biol Chem* **283**:5069–5080.
Ozalp C, Szczesna-Skorupa E, and Kemper B (2005) Bimolecular fluorescence complementation analysis of cytochrome p450 2c2, 2e1, and NADPH-cytochrome p450 reductase molecular interactions in living cells. *Drug Metab Dispos* **33**: 1382–1390.
Perera R, Sono M, Sigman JA, Pfister TD, Lu Y, and Dawson JH (2003) Neutral thiol as a proximal ligand to ferrous heme iron: implications for heme proteins that lose cysteine thiolate ligation on reduction. *Proc Natl Acad Sci USA* **100**:3641–3646.
Phillips JC, Braun R, Wang W, Gumbart J, Tajkhorshid E, Villa E, Chipot C, Skeel RD, Kalé L, and Schulten K (2005) Scalable molecular dynamics with NAMD. *J Comput Chem* **26**:1781–1802.
Praporski S, Ng SM, Nguyen AD, Corbin CJ, Mechler A, Zheng J, Conley AJ, and Martin LL (2009) Organization of cytochrome P450 enzymes involved in sex steroid synthesis: protein-protein interactions in lipid membranes. *J Biol Chem* **284**:33224–33232.
Reed JR and Backes WL (2017) Physical studies of P450-P450 interactions: predicting quaternary structures of P450 complexes in membranes from their x-ray crystal structures. *Front Pharmacol* **8**:28.
Reed JR, Connick JP, Cheng D, Cawley GF, and Backes WL (2012) Effect of homomeric P450-P450 complexes on P450 function. *Biochem J* **446**:489–497.
Rydberg P, Olsen L, Norrby PO, and Ryde U (2007) General transition-state force field for cytochrome P450 hydroxylation. *J Chem Theory Comput* **3**:1765–1773.
Sabat J, Stuehr DJ, Yeh SR, and Rousseau DL (2009) Characterization of the proximal ligand in the P420 form of inducible nitric oxide synthase. *J Am Chem Soc* **131**:12186–12192.
Schoch GA, Yano JK, Wester MR, Griffin KJ, Stout CD, and Johnson EF (2004) Structure of human microsomal cytochrome P450 2C8. Evidence for a peripheral fatty acid binding site. *J Biol Chem* **279**:9497–9503.
Schwarz D, Pirrwitz J, Meyer HW, Coon MJ, and Ruckpaul K (1990) Membrane topology of microsomal cytochrome P-450: saturation transfer EPR and freeze-fracture electron microscopy studies. *Biochem Biophys Res Commun* **171**:175–181.
Scott EE, He YA, Wester MR, White MA, Chin CC, Halpert JR, Johnson EF, and Stout CD (2003) An open conformation of mammalian cytochrome P450 2B4 at 1.6-A resolution. *Proc Natl Acad Sci USA* **100**:13196–13201.
Shing B, Singh S, Podust LM, McKerrow JH, and Debnath A (2020) The antifungal drug isavuconazole is both amebicidal and cysticidal against *Acanthamoeba castellanii*. *Antimicrob Agents Chemother* **64**:e02223-–19.
Siddiqui R and Khan NA (2012) Biology and pathogenesis of *Acanthamoeba*. *Parasit Vectors* **5**:6.
Šrejber M, Navrátilová V, Paloncýová M, Bazgier V, Berka K, Anzenbacher P, and Otyepka M (2018) Membrane-attached mammalian cytochromes P450: an overview of the membrane's effects on structure, drug binding, and interactions with redox partners. *J Inorg Biochem* **183**:117–136.
Sun L, Wang Z, Jiang H, Tan X, and Huang Z (2010) Novel conformational transitions of human cytochrome P450 2C8 during thermal and acid-induced unfolding. *Chin J Chem* **28**:1491–1502.
Sun Y, Zeng W, Benabbas A, Ye X, Denisov I, Sligar SG, Du J, Dawson JH, and Champion PM (2013) Investigations of heme ligation and ligand switching in cytochromes p450 and p420. *Biochemistry* **52**:5941–5951.
Szczesna-Skorupa E, Mallah B, and Kemper B (2003) Fluorescence resonance energy transfer analysis of cytochromes P450 2C2 and 2E1 molecular interactions in living cells. *J Biol Chem* **278**:31269–31276.
Thomson S, Rice CA, Zhang T, Edrada-Ebel R, Henriquez FL, and Roberts CW (2017) Characterisation of sterol biosynthesis and validation of 14α-demethylase as a drug target in Acanthamoeba. *Sci Rep* **7**:8247.
Vieira DF, Choi JY, Calvet CM, Siqueira-Neto JL, Johnston JB, Kellar D, Gut J, Cameron MD, McKerrow JH, Roush WR, et al. (2014a) Binding mode and potency of N-indolyloxopyridinyl-4-aminopropanyl-based inhibitors targeting *Trypanosoma cruzi* CYP51. *J Med Chem* **57**:10162–10175.
Vieira DF, Choi JY, Roush WR, and Podust LM (2014b) Expanding the binding envelope of CYP51 inhibitors targeting *Trypanosoma cruzi* with 4-aminopyridyl-based sulfonamide derivatives. *ChemBioChem* **15**:1111–1120.
Von Wachenfeldt C and Johnson EF (1995) Structures of eukaryotic cytochromes P450, in *Cytochrome P450: Structure, Mechanism, and Biochemistry* (Ortiz de Montellano PR ed) pp 183–223, Plenum Press, New York.
von Wachenfeldt C, Richardson TH, Cosme J, and Johnson EF (1997) Microsomal P450 2C3 is expressed as a soluble dimer in *Escherichia coli* following modification of its N-terminus. *Arch Biochem Biophys* **339**:107–114.
Wang A, Savas U, Hsu MH, Stout CD, and Johnson EF (2012) Crystal structure of human cytochrome P450 2D6 with prinomastat bound. *J Biol Chem* **287**: 10834–10843.
Zhou W, Debnath A, Jennings G, Hahn HJ, Vanderloop BH, Chaudhuri M, Nes WD, and Podust LM (2018) Enzymatic chokepoints and synergistic drug targets in the sterol biosynthesis pathway of *Naegleria fowleri*. *PLoS Pathog* **14**:e1007245.
Zhou W, Ramos E, Zhu X, Fisher PM, Kidane ME, Vanderloop BH, Thomas CD, Yan J, Singha U, Chaudhuri M, et al. (2019) Steroidal antibiotics are antimetabolites of *Acanthamoeba* steroidogenesis with phylogenetic implications. *J Lipid Res* **60**:981–994.

Address correspondence to: Larissa M. Podust, Pharmaceutical Sciences Bldg., PSB 2226, University of California San Diego, 9500 Gilman Dr., La Jolla, CA 92093. E-mail: lpodust@health.ucsd.edu